THE ASTROPHYSICAL JOURNAL, 401:L69–L73, 1992 December 20

HUBBLE SPACE TELESCOPE IMAGING OF DISTANT GALAXIES: 4C 41.47 AT $z = 3.8$

G. K. MILEY
Sterrewacht, Postbus 2513, 2300 RA Leiden, The Netherlands
K. C. CHAMBERS
Institute for Astronomy, 2680 Woodlawn Drive, Honolulu, HI 96822
W. J. M. VAN BREUGEL
University of California, Institute of Geophysics and Planetary Physics, L-413, Lawrence Livermore Laboratory, P.O. Box 808 Livermore, CA 94459
AND
F. MACCHETTO
Space Telescope Science Institute, 3700 San Martin Drive, Baltimore, MD 21218[1]
Received 1992 August 28; accepted 1992 October 1

ABSTRACT

The *Hubble Space Telescope* has been used to image the continuum emission from 4C 41.17 at $z = 3.8$, the most distant galaxy known. The galaxy was detected with good signal-to-noise ratio and was spatially resolved at the 0".1 (440 pc) *HST* resolution. The measured integrated flux density is in good agreement with the ground-based value ($R \sim 22$). About 35% of this emission is in the form of a high brightness clumpy region extending by about 0".5 (1.7 kpc), whose morphology is remarkably similar to that of the radio components. A fainter more diffuse region of optical emission extends westward from the center of the nuclear complex for about 1".2 (5.3 kpc) out along the radio axis.

The clumpiness of the optical emission and its close correspondence with the radio structure on the subkiloparsec scale is discussed in the light of current models for high-redshift galaxies. Our observations imply that the material in the center of this galaxy is clumpy on the subkiloparsec scale. If the emission is stellar, the luminosities are consistent with a mass of about $10^{10}\ M_\odot$ of stars in each ≤ 500 pc clump.

Subject headings: early universe — galaxies: active — galaxies: formation — galaxies: structure — radio continuum: galaxies

1. INTRODUCTION

4C 41.17 is a radio source associated with the most distant galaxy known to date, at a redshift of 3.8 (Chambers, Miley, & van Breugel 1990). The radio spectrum is ultrasteep, with an index of -1.3. Its optical spectrum shows bright Lyman-alpha, faint C IV λ1549, and a continuum with a sharp cutoff blueward of Lyman-alpha. The observed optical/infrared continuum and Lyman-alpha are extended and closely related morphologically to the radio emission. There is a Lyman-alpha halo which extends by at least 15" (70 kpc) along the radio axis.

The optical/infrared continuum emission from 4C 41.17 is relatively bright, with integrated magnitudes of 21.7, 21.8, and 18.6, respectively, in the R, I, and K bands, and $R = 23.8$ in a 1".2 × 1".2 area at the peak. Because of its large distance and high brightness, we chose 4C 41.17 as one of two objects with which to carry out a pilot project to investigate distant galaxies with the *HST*. Although distant galaxies were originally among the prime targets for the *HST*, the aberration problems cast doubt as to whether they could be usefully detected. Here, we present the results for 4C 41.17. Imaging of the other distant radio galaxy, 4C 28.58 at a redshift of 2.9, will be presented elsewhere.

At $z = 3.8$, the conversion from observed to intrinsic parameters is highly dependent on the cosmological model adopted. In this *Letter*, unless otherwise stated, we shall assume a Hubble constant of $H_0 = 75$ km s^{-1} Mpc^{-1}, and a deceleration parameter of $q_0 = 0.5$, giving a scale factor of 0".1 = 440 pc.

[1] Affiliated to the Astrophysics Division, Space Science Department, European Space Agency

2. *HST* OBSERVATIONS AND REDUCTION

The *HST* observations were carried out in five separate 2400 s exposures on 1992 January 15 with the Wide Field Camera (WFC) through the F702W filter. The galaxy was placed close to the center of WFC1. There are two bright stars within 1' of the target. To prevent "bleeding" from these stars, the observing time constraints were chosen to accept only CCD orientations for which verticals through the star images on the CCD were far from the target.

Data calibration and reduction were carried out using the IRAF/STSDAS image processing system. The data from the Post Operation Data Processing System (the pipeline) was recalibrated using the best flat field available for the F702W filter as of 1992 March (c191513rw). Inspection of this flat field showed no severe features in the vicinity of the target. All five sets of observations were combined using an algorithm that rejected 5 σ points, thereby eliminating most of the cosmic-ray events. To simplify subsequent processing, a 256 by 256 region around the target was extracted. Next, remaining cosmic-ray events and two bad columns were marked manually and their effects removed. The local background was then subtracted by fitting a low-order two-dimensional polynomial function.

Deconvolution of the data was performed using the Richardson-Lucy algorithm (e.g., Lucy 1974; Lucy & Baade 1989; Snyder 1990; White 1990) as implemented in STSDAS. First the theoretical point-spread function at the position of the

target was computed using the Telescope Image Modeling routines (TIM) in STSDAS. A grid which is a factor of 2 finer than the original WFC (undersampled) image was used. The image was then interpolated to the finer grid of the synthesized point-spread function (pixel separation 0".05). A 40 iteration deconvolution was carried out. Subsequent iterations were found to result in little further change to the model brightness distribution.

3. RESULTS

Figure 1 (Plate L5) shows the "raw" image from WFC1 of the area surrounding 4C 41.17. It has been rotated by 209°.1 so that the north-south direction is vertical. This should be compared with the radio contour maps from Chambers et al. (1990). An enlargement of the center of the *HST* image after deconvolution is shown in Figures 2 (Plate L6) (gray scale) and 3 (contour). Note that the deconvolved images have not been rotated. Emission from the galaxy is seen over a distance of at least 3".5 (15 kpc) in a position angle of 260° ± 5°. Four peaks are clearly visible both on the deconvolved and raw *HST* images and are denoted in order of right ascension by H1, H2, H3, and H4. They are almost colinear in a position angle of 256° ± 5°. The effect of the deconvolution, as expected, is to sharpen the brightness distributions.

Three of these peaks, H2, H3, and H4, are concentrated in a region 0".5 (2 kpc) in a position of 250°. This corresponds very closely with the separation and position angle of the brightest radio peaks B2 and B3 in Chambers et al. (1990), 0".58 in PA 249° (Fig. 3).

3.1. *Astrometry*

It is important to determine the absolute positions of the optical component as accurately as possible in order that the *HST* image can be compared with the VLA radio image. Of particular interest is whether the various optical and radio components are related.

With this goal, preliminary astrometry was carried out on the larger "raw" combined image. The pixel positions corresponding to the peak intensities of the target were measured as well as the positions of several stars in the field. Corrections for relative internal distortions were applied using a program developed at the STScI by Ewald and Gimozzi. The corrected pixel coordinates were converted to celestial coordinates using the XY2RD program in STSADAS. The J2000 coordinates derived for H2 and H4 were found to be within 1".5 of the precessed coordinates of the radio core components B2 and B3. The data are presented in Table 1.

There are indications that these "raw" uncorrected positions have a systematic error of ~1".5. A star was present on the WFC image which was also on the ground-based CCD image of Chambers et al. and designated by them as "Star y." Chambers et al. measured its position accurately using the NRAO plate measuring machine and derived its (1950) position. When precessed to epoch 2000, this NRAO "POSS" position for Star y differed by about 1".5 from the WFC position. Since the WFC position of Star y was measured in exactly the same manner as the components of 4C 41.17, the same positional shift was applied to the WFC positions of the components of 4C 41.17 to bring them onto the more accurate POSS frame. Applying this correction to the *HST* positions, results in the *HST* peaks, H2 and H4, coinciding with the radio components, B2 and B3, to better than 0".1. Note that this good agreement is fortuitous; there is an uncertainty between the optical and radio frames of reference of several tenths of an arcsecond. The positional information is tabulated in Table 1.

TABLE 1

POSITIONAL INFORMATION (J2000)

Object	Right Ascension	Declination	Offset
Radio Components:			
B1	06^{h}50^{m}52^s.09	+41°30'30".6	
B2	06 50 51.19	+41 30 31.1	
B3	06 50 52.24	+41 30 31.3	...
Star y (WFC)	06 50 53.17	+41 30 39.5	
Star y (POSS)	06 50 53.14	+41 30 42.0	
Star y (POSS-WFC)	−0.03	+1.5	1".5
Component H2 (WFC)	06 50 52.23	+41 30 29.6	
Component H2 (POSS)	06 50 52.20	+41 30 31.1	
Radio B2-Optical H2 (POSS	−0.01	0.0	0.1
Component H3 (WFC)	06 50 52.25	+41 30 29.8	
Component H3 (POSS)	06 50 51.17	+41 30 31.3	
Component H4 (WFC)	06 50 52.27	+41 30 29.8	
Component H4 (POSS)	06 50 52.24	+41 30 31.3	
Radio B3-Optical H4 (POSS)	0.00	0.0	0.0

The arguments presented here indicate that the region of maximum optical intensity (H2, H3, H4) coincides with and is closely related morphologically to the region of maximum radio intensity (B2, B3). This may well contain the nucleus of 4C 41.17, although there is evidence that the position of the optical peak changes with color (Chambers et al. 1990).

3.2. *Photometry*

The number of counts produced by the various components was determined using the box-integration task IMSTAT in IRAF. This was done both on the raw combined image and on the deconvolved image, and the local background was determined on equivalent areas and subtracted. Relative photometric calibration between the deconvolved and raw images was determined by repeating the same process on the star which was present on both.

Conversion of counts to absolute photometric units was done by dividing the counts (*DN*) by the total exposure time, *t*, and multiplying by a factor to convert between *DN* and *R*-magnitude. The conversion factor was obtained in two ways. First, the data given in the Wide Field Camera/Planetary Camera Science Verification Report for the F702W filter, together with the calibration data from Harris et al. (1991), was used to obtain *R* magnitudes and the conversion to janskys was carried out with the zero-point value given by Zombek (1990). Second, the conversion factor was obtained from Version 3.0 of the *HST* WF and PC Instrument Handbook. The conversion factors from the two sources differed by 7%. We used the mean of the two methods, namely,

$$R = 22.592 - 2.5 \log (DN/t)$$

and

$$F_\nu \text{ (Jy)} = 2.61 \times 10^{-6 \times (DN/t)} .$$

The resultant photometric data are shown in Table 2, for the whole nuclear region, as well as for the individual components designated in Figure 3. They have a formal uncertainty of ±10%, but the definition of a "component" is to some extent subjective. The *R* magnitudes of 22.2 for the central 5" × 5"

TABLE 2

PHOTOMETRY OF 4C 41.17

Component	R	μJy
Central 5″ × 5″	22.2	3.62
Central 1″ × 1″	23.3	1.34
Component H1 2″ × 2″	24.1	0.68
Component H1 (peak).....	26.0	0.08
Component H2	24.4	0.47
Component H3	24.7	0.34
Component H4	24.5	0.43

NOTE.—Components ordered from west to east, H1, H2, H3, H4.

region is consistent with the value of 22.0 ± 0.5 quoted by Chambers et al. (1990) for the same region of the galaxy.

A question of profound relevance to the interpretation concerns the relative contribution in the image due to continuum emission compared with that due to Lyman-alpha. Chambers et al. (1990) find an equivalent width for Lyman-alpha of 1300 ± 200 Å for the peak emission visible on the ground-based image. The F702W filter will attenuate the response to Lyman-alpha by a factor of 20 and the half-intensity width (FWHM) of the filter is 1493 Å. We therefore estimate contamination from Lyman-alpha to be on average only about 1/70 of the continuum, although if the line is distributed differently from the continuum and if it is clumped, the relative line contribution might be significant in places. Here we shall assume that Figures 1, 2, and 3 represent the rest frame ultraviolet continuum emission of 4C 41.17 in the 1300–1600 Å region of the spectrum.

The radio-to-optical spectral indices of the coincident radio and optical knots (B2, H2) and (B3, H4) have been calculated between 14 GHz and 6900 Å on the basis of the *HST* photometry and the radio data in Chambers et al. (1990). The derived indices are -0.78 and -0.83, respectively, with a formal uncertainty of 0.05, compared with -1.35 ± 0.16 for the (B2, B3) complex between 5 and 14 GHz. Hence, the radio/optical spectra are significantly flatter than the radio ones and the optical flux of the knots are a factor of ~ 300 larger than the value given by extrapolation of their radio (synchrotron) spectrum.

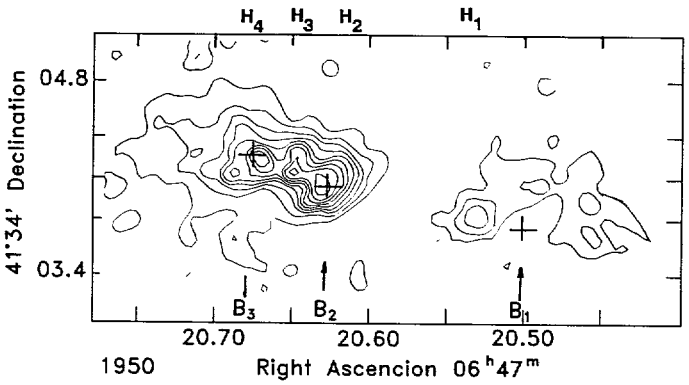

FIG. 3.—A linear contour representation of the deconvolved *HST* image (Fig. 1). The positions of the radio components B1, B2, and B3 (Fig. 2) are marked by crosses. The right ascensions of the *HST* components denoted by H1, H2, H3, and H4 in the text are indicated. Note that there is an uncertainty of a few tenths of an arcsecond between the radio and optical astrometric reference frames.

3.3. *Morphologies*

4C 41.17 shows extremely clumpy structure on the scale of the *HST* resolution. Although the emission extends for more than 3″.5, the structure is concentrated, with about one-third of the flux originating from a high-brightness region extending by about 0″.5, which we presume to contain the nucleus of 4C 41.17. This nuclear region is highly clumped on the scale of the *HST* resolution; at least three peaks of emission are discernible. A fainter, more diffuse region of optical emission extends from about 1″.2 (5.3 kpc) west of the center of the nuclear complex outward along the radio axis.

One of the most striking results from our *HST* image is the correspondence between the optical and radio images. The orientation of the nuclear emission of the optical and the radio agree to within about a degree, and the extent is also comparable. The peaks of the *HST* nuclear emission, H2 and H4 can be identified with radio components, B2 and B3. The comparable resolution 14 GHz radio map is noise-limited, and it is possible that a deeper radio map may reveal a counterpart of the third optical peak, H3.

The position angle of the radio structure is slightly (but significantly) different within the nuclear complex (250° from B3 to B2) outward toward the west (256° from B3 to B1). This curvature of $7° \pm 2°$ toward the northwest is mirrored in the optical image. In the radial direction, the optical peak H1 does not correspond exactly with the nominal radio peak of B1. However, in view of the poor signal-to-noise ratio and large extent of these components, the component peak intensities are ill defined in the radial direction and the lack of exact coincidence is not significant.

4. DISCUSSION

During the last decade, considerable evidence has emerged that the optical emission from distant galaxies is closely related to the radio emission. Unlike the situation for nearby radio galaxies, the radio emission is roughly aligned with the optical/infrared continuum emission (for $z > 0.6$) (Chambers, Miley, & van Breugel 1987; McCarthy et al. 1987). Several models have been proposed or considered to account for the alignment effect (e.g., see Chambers & Miley 1989). The most viable ones are star formation stimulated by the radio jet as it propagates outward from the nucleus (De Young 1981; Chambers et al. 1987; McCarthy et al. 1987; Rees 1989; Begelmann & Cioffi 1989; De Young 1989), and scattering of light from a hidden quasar by electrons or dust (Tadhunter, Fosbury, & di Sergio Aligheri 1989; Fabian 1989).

Recently, Eales (1992) has proposed a new model for the alignment effect. This postulates (1) the radio luminosity increases with ambient density and (2) distant galaxies have an anisotropic density distribution, elongated along their major axes. Flux-limited radio surveys would then systematically detect radio sources with high luminosity, the aligned objects.

What implications do our *HST* data have for these various models? Our most important new results are (1) the clumpiness of the optical emission from 4C 41.17 on the subkiloparsec scale, (2) the photometry of the clumps, and (3) the close correspondence of the optical and radio emission on scales ranging from 0″.1 to 3″.5 (400 pc to 15 kpc). Let us consider the starburst, scattering, and anisotropic density models.

4.1. *Jet-induced Star Formation*

In the starburst model, the clumps represent giant clusters of stars formed in regions of high gas density as the jet propagates

outward from the nucleus. Chambers et al. (1990) showed that the integrated spectral energy distribution for 4C 41.17 is consistent with a relatively young age for the galaxy of $< 3 \times 10^8$ yr in which the bulk of the stars were formed in $< 10^8$ yr, with about $5 \times 10^{11}\ M_\odot$ in stars ($H = 50$ km s^{-1} Mpc^{-1}). The flux density of the nuclear clumps seen by the *HST* ($\sim 0.4\ \mu$Jy) is about 70% of the total flux density in *R* band for 4C 41.17. Scaling on the assumption that the clumps have similar spectral energy distributions would give a total mass in stars of about $1.5 \times 10^{10}\ M_\odot$ in each ≤ 500 pc–sized clump. Because ground-based work indicates that there are color gradients in the optical emission from 4C 41.17, color information on the resolution of the *HST* is needed to refine these estimates.

4.2. *Scattering*

Although there are problems with explaining the total aligned optical/infrared continuum from radio galaxies, by scattering alone, the optical polarization detected from a few bright radio galaxies suggest that some scattering occurs, at least in the rest frame ultraviolet. In the pure scattering model, the clumps are lumps of gas or dust being "lit up" by the invisible quasar.

One result relevant to this picture concerns the close resemblance between the radio and optical morphologies on the kiloparsec scale, and in particular the hint of similar curvature between the radio and *HST* images. The orientation in both wavelength regimes changes by $7° \pm 2°$ between the central 2 kpc and the outer 10–15 kpc. This is a small, but significant difference. It is difficult to explain the presence of detailed similarities between the optical and radio properties (brightness and curvature) on the basis of the simple scattering model. In this picture the photon beam cone and the narrower radio jet are emitted in the same direction. Bends in the radio jet are produced either by shear of the ambient medium or by changes in the direction of the ejection axis (e.g., precession). Apparent bends in the optical emission could be produced either by nonuniformities in the distribution of the scattering medium across the cone, or changes in the cone direction. There is no obvious reason why the nonuniformities in the ISM would follow the bending of the radio jet. Although precession of the central machine would cause both the photon cone and the radio jet to change direction, the bending would coincide only if the radio source propagated outward at the same speed as the photons (velocity of light) instead of about 5% of this as implied by conventional radio source models (Leahy 1991). In the case of 4C 41.17, the correspondence of the radio and optical curvature could be fortuitous. However, if this effect is observed in other distant radio galaxies and is demonstrated to be a general property, it would present difficulties for the simple scattering model of the alignment effect.

4.3. *Anisotropically Enhanced Radio Emission*

On the basis of this model, the large-scale optical axis would be aligned along the radio source. However, there is no reason that the optical emission should be clumpy and why these clumps should so closely mimic the radio emission on the kiloparsec nuclear scale. Also, the radio properties of 4C 41.17 are difficult to explain by means of this model. One would expect that on the scale of the radio sources (~ 60 kpc) radial differences in the density and other properties of the medium through which the jet propagates would dominate any azimuthal effects. For example, one would expect huge differences in density should exist between the kiloparsec-scale region surrounding the nucleus and the outer part of the galaxy where the radio hot spots are located. But the radio luminosity in the central (dense) 2 kpc of 4C 41.17 is comparable to the luminosity in the outer hot spots 30 kpc away, indicating that ambient density is not an important factor governing the radio luminosity of jets.

5. CONCLUSIONS AND FUTURE WORK

Our *HST* image of 4C 41.17 demonstrates that, despite its poor aberrated health, the *HST* can be used to image a galaxy at a redshift of almost 4, corresponding to an epoch of about only 10% of the present age of the universe. The close correspondence between the optical *HST* image and the radio structure means that the mechanism responsible for the alignment effect works efficiently within the central region of the galaxy. About one-third of the emission from 4C 41.17 arises from a clumpy elongated region of size about 0.5×2 kpc. For most viable scenarios, the clumpiness in the emission implies an inhomogeneity in the medium of the inner region of the galaxy. If these clumps are due to stars, models would indicate each clump contains a giant cluster of about $10^{10}\ M_\odot$ stars in a region about 500 pc in size. The detailed morphological similarities between the kiloparsec-scale optical and radio emission presents problems for the scattering and enhanced-radio models.

Clearly, further investigation of 4C 41.17 with the *HST* is warranted. During the next year we expect to obtain a picture of 4C 41.17 in the F569W filter which is centered close to Lyman-α. Additional *HST* images of this galaxy in other filters would enable the colors of the clumps to be determined and compared with models.

This pilot study has been successful. There are now more than 60 galaxies known with redshifts larger than 2. On the basis of our images of 4C 41.17 and 4C 28.58 (Chambers et al. 1992), the nuclear structures in the majority of these are well matched to mapping by the *HST*, despite its aberration. After WF/PC2 has been installed and the *HST* optics corrected, much of the faint outer structure of the galaxies should be observable. Expectations are now high that individual and statistical studies of the morphologies of samples of distant radio galaxies with the *HST* can give information on the processes occurring in the most extreme active galaxies, probe the environment in the early universe, and constrain cosmological models.

We thank Dan Golombek, Diane Gilmore, and Matt McMaster for their exemplary help in carrying out the data reduction. We are also grateful to Shawn Ewald, Roberto Gilmozzi, Bob Hanisch, John Mackenty, Rob van Ojik, and Huub Rottgering for useful discussions and the referee for useful comments. We acknowledge partial support from the Netherlands Space Research Organisation, the Netherlands Foundation for Research in Astronomy, and grants from the NASA *HST* GO program, the NATO Research program, and the European Economic Community. The National Radio Astronomy Observatory is operated by AUI and the Kitt Peak National Observatory by AURA, both under contract from the National Science Foundation. The work of W. v. B. was performed at IGPP/LLNL under the auspices of the US Department of Energy under Contract W-7405-ENG-48.

REFERENCES

Begelman, M. C., & Cioffi, D. F. 1989, ApJ, 345, L21
Chambers, K. C., & Miley, G. K. 1989, in The Evolution of the Universe of Galaxies: The Edwin Hubble Centennial Symposium, ed. R. G. Kron (ASP Conf. Ser. 10), 373
Chambers, K. C., Miley, G. K., & van Breugel, W. J. M. 1987, Nature, 329, 604
———. 1990, ApJ, 363, 21
Chambers, K. C., Miley, G. K., van Breugel, W. J. M., & Macchetto, F. 1992, in preparation
De Young, D. S. 1981, Nature, 293, 43
———. 1989, ApJ, 342, L59
Eales, S. A. 1992, ApJ, 397, L19
Fabian, A. 1989, MNRAS, 243, 1P
Harris, H. C., et al. 1991, AJ, 101, 677
Leahy, P. 1991, in Beams and Jets in Astrophysics, ed. P. A. Hughes (Cambridge: Cambridge Univ. Press), 100
Lucy, L. 1974, AJ, 79, 745
Lucy, L. B., & Baade, D. 1989, in Proc. 1st ESO-ECF Data Analysis Workshop, ed. P. Grosbol, R. H. Warmels, & F. Murtagh (Garching: ESO), 219
McCarthy, P. J., van Breugel, W. J. M., Spinrad, H., & Djorgovski, S. 1987, ApJ, 321, L29
Rees, M. J. 1989, MNRAS, 239, 1P
Snyder, D. L. 1990, in The Restoration of *HST* Images and Spectra, ed. R. L. White & R. J. Allen (Baltimore: STScI), 56
Tadhunter, C. N., Fosbury, R. A. E., & di Sergio Aligheri, S. 1989, in Proc. Como Conference on BL Lac Objects: 10 Years After, ed. L. Marasci (Berlin: Springer-Verlag), 79
White, R. L. 1990, in The Restoration of *HST* Images and Spectra, ed. R. L. White & R. J. Allen (Baltimore: STScI), 139
Zombek, M. V. 1990, Handbook of Space Astronomy and Astrophysics, 2d ed. (Cambridge: Cambridge Univ. Press), 100

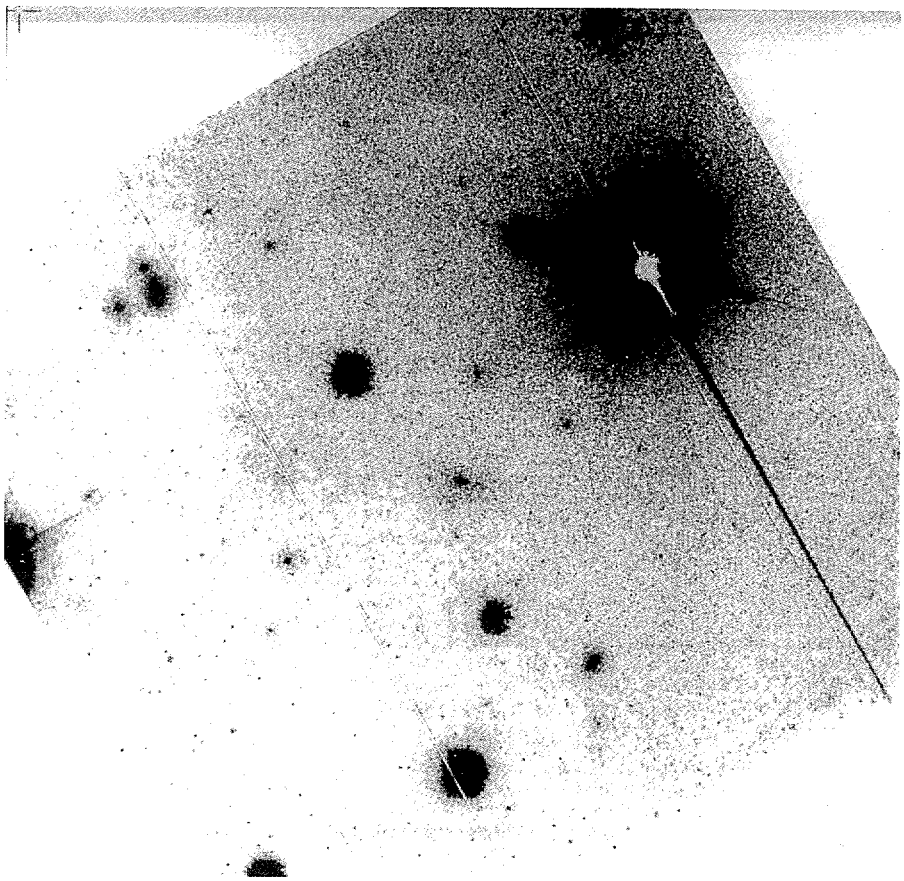

FIG. 1.—The WFC1 image of a 1'.3 × 1'.3 region surrounding 4C 41.17. The 800 × 800 pixel image is the result of combining five separate 2400 s images (total exposure time 3 hr 20 minutes). The image has been rotated, so that north is vertical. The fuzzy object near the center of the field is the galaxy associated with 4C 41.17.

MILEY et al. (see 401, L70)

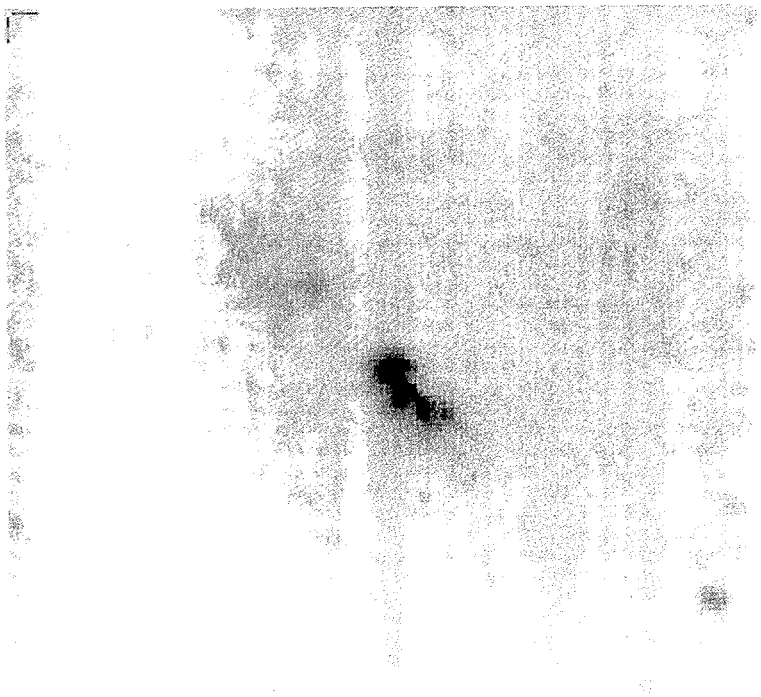

FIG. 2*a*

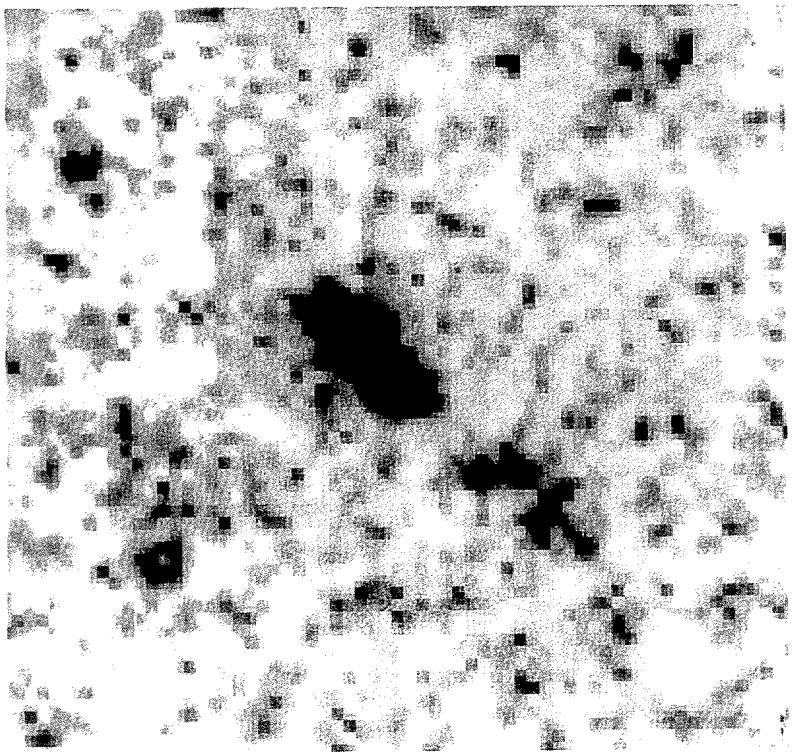

FIG. 2*b*

FIG. 2.—Gray-scale representations of a 25".6 × 25".6 subarray from the *HST* image containing 4C 41.17 (Fig. 1) after a 40 iteration Lucy-Richardson deconvolution (see text). North is at an angle of 150°.9 measured anticlockwise from the vertical.